







The plant-specific DDR factor SOG1 increases chromatin mobility in response to DNA damage

Anis Meschichi¹ , Lihua Zhao¹ , Svenja Reeck², Charles White³ , Olivier Da Ines³ , Adrien Sicard¹, Frédéric Pontvianne⁴  & Stefanie Rosa^{1,*} 

Abstract

Homologous recombination (HR) is a conservative DNA repair pathway in which intact homologous sequences are used as a template for repair. How the homology search happens in the crowded space of the cell nucleus is, however, still poorly understood. Here, we measure chromosome and double-strand break (DSB) site mobility in *Arabidopsis thaliana*, using *lacO/LacI* lines and two GFP-tagged HR reporters. We observe an increase in chromatin mobility upon the induction of DNA damage, specifically at the S/G2 phases of the cell cycle. This increase in mobility is lost in the *sog1-1* mutant, a central transcription factor of the DNA damage response in plants. Also, DSB sites show particularly high mobility levels and their enhanced mobility requires the HR factor RAD54. Our data suggest that repair mechanisms promote chromatin mobility upon DNA damage, implying a role of this process in the early steps of the DNA damage response.

Keywords *Arabidopsis*; chromatin mobility; DNA damage; DSBs; SOG1

Subject Categories Chromatin, Transcription & Genomics; DNA Replication, Recombination & Repair

DOI 10.15252/embr.202254736 | Received 28 January 2022 | Revised 30 September 2022 | Accepted 5 October 2022 | Published online 24 October 2022
EMBO Reports (2022) 23: e54736

Introduction

Genome integrity is constantly threatened by internal and external stressors. Therefore, in response to DNA damage, eukaryotic organisms evolved elaborate DNA-damage response (DDR) systems that comprise DNA-damage signaling processes, DNA repair, and other responses such as cell death and control of cell division (Yoshiyama *et al.*, 2013b). Among the different types of DNA damage, double-strand breaks (DSBs) are particularly harmful to cells, leading potentially to chromosome rearrangements or loss of entire chromosome arms (van Gent *et al.*, 2001). DSBs can be repaired by two main pathways, nonhomologous end joining (NHEJ) and homologous recombination (HR; Jackson, 2002; West *et al.*, 2004). NHEJ is

achieved by stabilization and re-ligation of broken DNA ends, often with loss or mutation of bases. HR is a more complex and more conservative mechanism in which intact homologous sequences are used as a template for repair. HR most commonly occurs in S/G2 phases of the cell cycle in eukaryotic cells when sister chromatids are present, although homologous donor templates present elsewhere in the genome can also be used (Johnson & Jasin, 2000; Li & Heyer, 2008; Goldfarb & Lichten, 2010). Despite the vast knowledge about the molecular players involved in DNA repair via HR, the mechanisms behind the search and recognition of homologous sequences (“homology search”) are still not well understood. In yeast, large-scale movements of DSBs have been identified following DSB induction (Oza *et al.*, 2009; Dion *et al.*, 2012; Ryu *et al.*, 2015; Schrank *et al.*, 2018). Yet, the precise functions of these movements remain unclear.

Plants are potentially subject to particularly high levels of DNA damage resulting from dependence on sunlight for energy and exposure to environmental stresses (Ries *et al.*, 2000; Lee *et al.*, 2012; Kawarazaki *et al.*, 2013; Küpper & Andresen, 2016; Zhao *et al.*, 2018). Moreover, plant development is mostly postembryonic with a late germline differentiation. Therefore, it is particularly interesting to understand the mechanisms that allow these organisms to cope with the constant assaults on their genome integrity. Indeed, plants have evolved a distinct DDR master regulator—SUPPRESSOR OF GAMMA RESPONSE 1 (SOG1). This transcription factor initiates a repair response by inducing genes involved in cell cycle arrest and repair, as well as in programmed stem-cell death in response to DNA damage (Yoshiyama *et al.*, 2009, 2013a; Bourbousse *et al.*, 2018). While the molecular processes involved in DDR pathway have been extensively characterized also in plants, little has been done to address how chromatin mobility changes in response to DNA damage and in particular to DSBs. Here, we have used locus tagging systems and HR reporter lines to study chromatin mobility upon genotoxic stress with the DSB inducer agent zeocin. We observed that in the presence of DSBs, both damaged and potentially undamaged loci increase the volume that they explore within the nuclear space. We showed that this increase in chromatin mobility occurs specifically during the G2 phase of the cell cycle and depends on the plant-specific DDR master regulator SOG1, implying

1 Plant Biology Department, Swedish University of Agricultural Sciences, Uppsala, Sweden

2 John Innes Centre, Norwich Research Park, Norwich, UK

3 Institut Génétique Reproduction et Développement (iGRéD), Université Clermont Auvergne, UMR 6293, CNRS, U1103 INSERM, Clermont-Ferrand, France

4 CNRS, Laboratoire Génome et Développement des Plantes (LGDP), Université de Perpignan Via Domitia, Perpignan, France

*Corresponding author. Tel: +46 18673324; E-mail: stefanie.rosa@slu.se

an important role for chromatin mobility during the early steps of the DNA damage response.

Results and Discussion

To measure chromatin mobility in plant cells, we used the *lacO*/LacI-GFP locus-tagging system (Matzke *et al.*, 2010, 2019; Fig 1A). For simplicity and to be consistent with previous studies, we will refer to the term chromatin mobility, even though we are measuring the mobility of individual foci at a given time. Foci mobility measurements were carried out using a mean square displacement (MSD) analysis. This analysis robustly measures the mobility of diffusing, fluorescently tagged chromosomal loci and provides kinetic parameters describing loci motion (Horigome *et al.*, 2015; Meschichi & Rosa, 2021). We first tested our setup by measuring “steady-state” chromatin mobility levels for cells in the division versus differentiation zones of the *Arabidopsis thaliana* (*Arabidopsis*) root (Fig 1B). Measurements of histone exchange had previously shown that cells at the division zone have a more dynamic chromatin state as compared to differentiated cells (Rosa *et al.*, 2014; Arai *et al.*, 2017). Consistently, we observed that chromatin mobility is also higher in cells from the division zone compared to cells from the differentiation zone (Fig 1C). The radius of constraint (Rc), which indicates the nuclear volume within which a fluorescent spot can move, was therefore significantly higher in cells from the division zone (Fig 1C). These results confirmed that our setup is suitable to unpick differences in chromatin mobility between cells. In *Arabidopsis* root, differences in nucleus size are often evident, not only between nuclei from the division and differentiated zones but also within the meristem itself. As such, we thought to verify if our MSD measurements would be affected by differences in nucleus size. Within the meristematic region from the root, cells have the same ploidy level (diploid), but nuclei of atrichoblast cells are considerably bigger than that of trichoblast cells (Fig 1D). Nevertheless, these two cell types show the same chromatin mobility and radius of constraint (Fig 1E), ruling out that the nuclear volume *per se* could affect overall chromatin mobility levels.

Because HR requires pairing of the broken DNA molecule with a homologous intact template, we tested whether *Arabidopsis* cells actively regulate chromatin mobility in response to DSBs. We induced DNA damage by incubating 6-day-old seedlings with the DSB inducer zeocin for 24 h (Fig 2A). This treatment led to the upregulation of the DDR-responsive genes *PARP1*, *RAD51*, and *BRCA1*, indicating that the HR was effectively stimulated (Appendix Fig S1A). This provided us with a system to induce different levels of DNA damage. We further focused our analysis on cells within the division zone since previous studies showed that the principal actors of HR, *RAD51* and *RAD54*, are mainly expressed in these cells (Da Ines *et al.*, 2013; Hirakawa *et al.*, 2017). MSD analysis revealed that *lacO*/LacI foci mobility was not changed upon low concentrations or shorter times of zeocin incubation but increased significantly with high concentrations of zeocin for 24 h (Fig 2B; Appendix Fig S2). We acknowledge that 170 μ M zeocin is a very high concentration, and many damage sites are induced simultaneously (Appendix Fig S3). While we cannot rule out that effects at other cellular processes may take place at this concentration, similar doses have been applied in other systems and are required to bring

the level of damage above a certain threshold that triggers the increase in chromatin mobility or to increase the probability of inducing a break near to *lacO* transgene (Seeber *et al.*, 2013). Importantly, the effect seen at the higher concentration was not due to DNA damage-induced programmed cell death as tested by PI staining (Appendix Fig S4). Only stem cells and their early descendants, which are known to be highly sensitive to DNA damage (Fulcher & Sablowski, 2009), showed PI-positive staining but not the epidermal cells used in our chromatin mobility analysis. We also tested another DSB inducer chemical, mitomycin C (MMC). A similar increase in chromatin mobility was observed in response to MMC treatment (Appendix Fig S5), showing that this is a general response to DSB induction.

In order to verify if the increase in chromatin mobility observed upon zeocin treatment was specific for the particular *lacO* insertion site in line112 or a response at the global chromatin level, we analyzed additional *lacO*/LacI lines with insertions at different chromosomal locations (Fig 2C). In control conditions, line 26 shows the same chromatin mobility as line 112, whereas line 107 showed significantly lower chromatin mobility and Rc (Appendix Fig S6). The lower mobility in line 107 could be linked to the transgene insertion at the subtelomeric region, known to physically interact at the nucleolar periphery in *Arabidopsis* (Armstrong *et al.*, 2001; Fransz *et al.*, 2002; Pontvianne *et al.*, 2016; Fig 2C). Upon treatment with high zeocin concentration, all lines showed a significant increase in chromatin mobility and Rc (Fig 2D and E), indicating that chromatin mobility increases globally in the nucleus in response to DNA damage. We also tested whether these results could be an artifact of the *lacO*/LacI system itself. For that, we performed the same experiments using another locus tagging system—the ANCHOR system (*ParB-parS*; Meschichi *et al.*, 2021; Fig 2F). The ANCHOR line showed a similar increase in chromatin mobility (Fig 2G).

Existing evidence in several systems shows that cell cycle arrest upon DNA damage is used by cells to facilitate DNA repair before cell division (Johnson & Jasin, 2000; Weimer *et al.*, 2016; Chang *et al.*, 2017; Hustedt & Durocher, 2017). Since DNA content and cohesion differ in different cell cycle phases, we sought to test if changes in cell cycle dynamics (i.e. the proportion of cells in different cell cycle phases) could explain the increased chromatin mobility observed in response to DNA damage. To test this hypothesis, we crossed the *lacO*/LacI (line 112) with the S/G2 reporter CDT1a::RFP (Yin *et al.*, 2014; Fig 3A and B). To first verify that this setup was working as expected, we quantified the ratio of cells in S/G2 in root epidermal cells treated with Hydroxyurea (HU), a drug known to block cells in S phase (Cools *et al.*, 2010; Singh & Xu, 2016). Indeed, we observed that there was a higher proportion of cells in S/G2 in HU samples (Fig 3C). Consistent with previous studies (Chen *et al.*, 2017), treatment with 10 μ M zeocin significantly increased the number of cells in S/G2 (Fig 3C). However, with the highest concentration of zeocin (170 μ M), the ratio of cells in S/G2 phase decreased to half in comparison with control conditions (Fig 3C), suggesting an accumulation of cells in G1. Thus, it became important to determine if G1 cells had different chromatin mobility compared to S/G2 cells. MSD analysis revealed that cells in the S/G2 phase (CDT1a-RFP positive cells) showed lower chromatin mobility than G1 cells (Fig 3D). Similarly, HU-treated cells showed lower chromatin mobility, most likely due to cells being arrested in

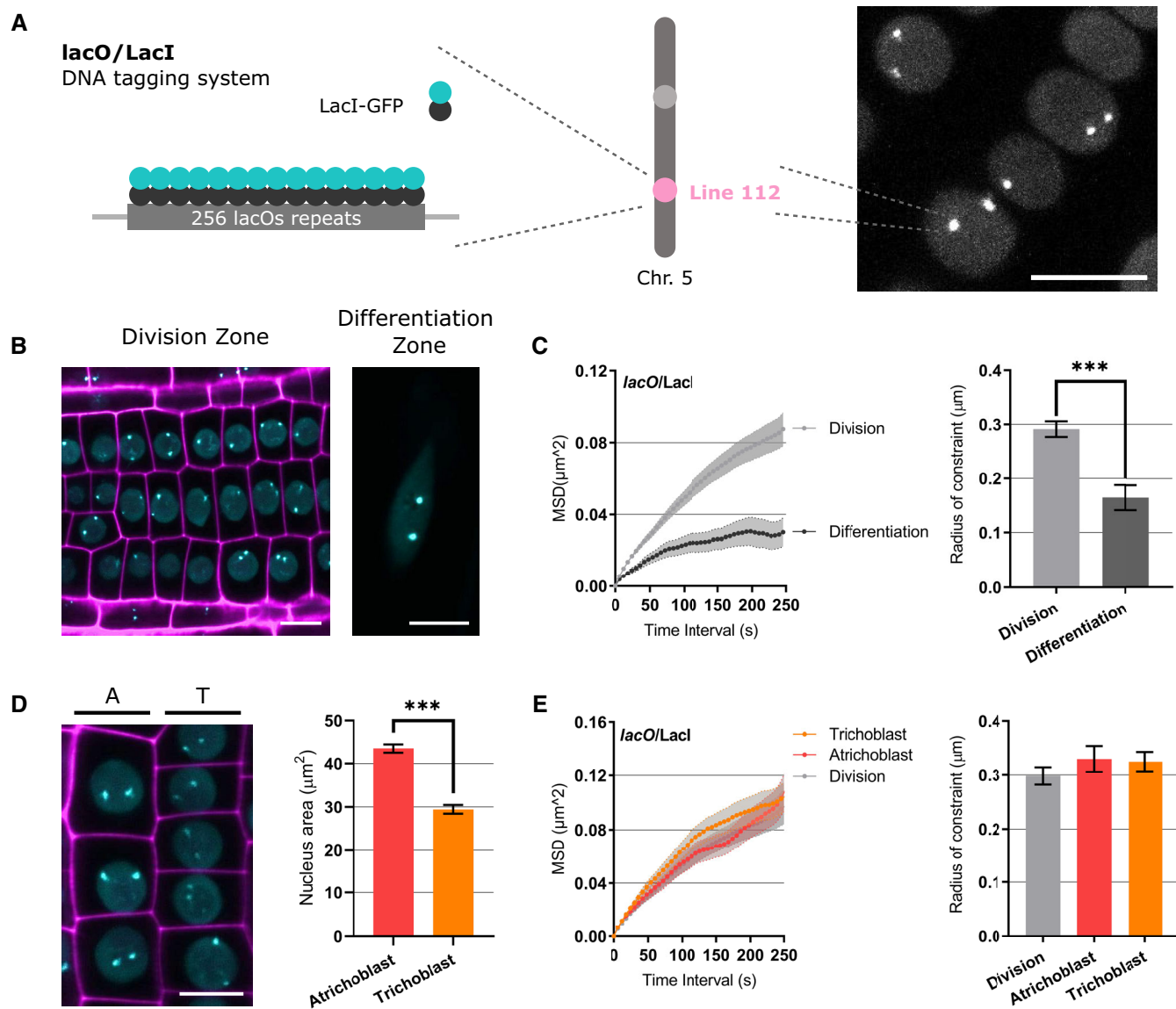


Figure 1. The mobility of *lacO* foci in different cell types in *Arabidopsis thaliana* root.

A Schematic representation of the *lacO/LacI* system. A *lacO* repeat array was integrated into chromosome 5 (line112) and detected by expression of the LacI protein fused to GFP. The image on the right corresponds to a z-projected image from root epidermal nuclei expressing the referred construct. Scale bar, 10 μm .

B Representative images of the *Arabidopsis* root epidermal cells in division (left image) and differentiation zone (right image) showing nuclear signal with *lacO/LacI* foci (cyan). Propidium iodide (PI) staining (magenta). Scale bar, 10 μm .

C Left: MSD analysis of *lacO/LacI* lines based on time-lapse experiments of nuclei in the division ($n = 116$ nuclei) and differentiated zone ($n = 21$ nuclei). 3D stacks were taken at 6 s intervals for 5 min. Right: The radius of constraint was calculated from MSD curves. Values represent means \pm SEM. Student's t-test, $***P < 0.001$.

D Left: Representative images of atrichoblast (A) and trichoblast (T) in the division zone showing nuclear signal with *lacO/LacI* foci (cyan). Propidium iodide (PI) staining (magenta). Scale bar, 10 μm . Right: Histogram of nuclear areas (μm^2) from atrichoblast and trichoblast cells. Atrichoblast ($n = 53$ nuclei); red, Trichoblast ($n = 57$ nuclei); orange. Values represent means \pm SEM. Student's t-test, $***P < 0.001$.

E Left: MSD analysis of *lacO/LacI* lines based on time-lapse experiments of nuclei in the atrichoblast ($n = 36$ nuclei) and trichoblast ($n = 61$ nuclei). Right: Radius of constraint calculated from MSD curves. Values represent means \pm SEM.

the S/G2 phase (Fig 3E). These results revealed that an accumulation of cells in G1 could potentially explain the increased mobility observed in response to DSBs. If this is the case, we hypothesized that we should not see differences when comparing cells at the same stage of the cell cycle with or without zeocin. We, therefore, measured the chromatin mobility specifically at G1 and S/G2, in control conditions and upon treatment with different concentrations of

zeocin. Consistent with previous studies in yeast (Dion *et al*, 2012; Cheblal *et al*, 2020), we observed a significant increase in chromatin mobility in cells at S/G2 after zeocin treatment, whereas cells in G1 did not show any significant change (Fig 3F and G). We concluded that the increased mobility observed in response to DNA damage at high zeocin concentrations (170 μM) could be both a result of an accumulation of cells in G1 and a specific increase in chromatin

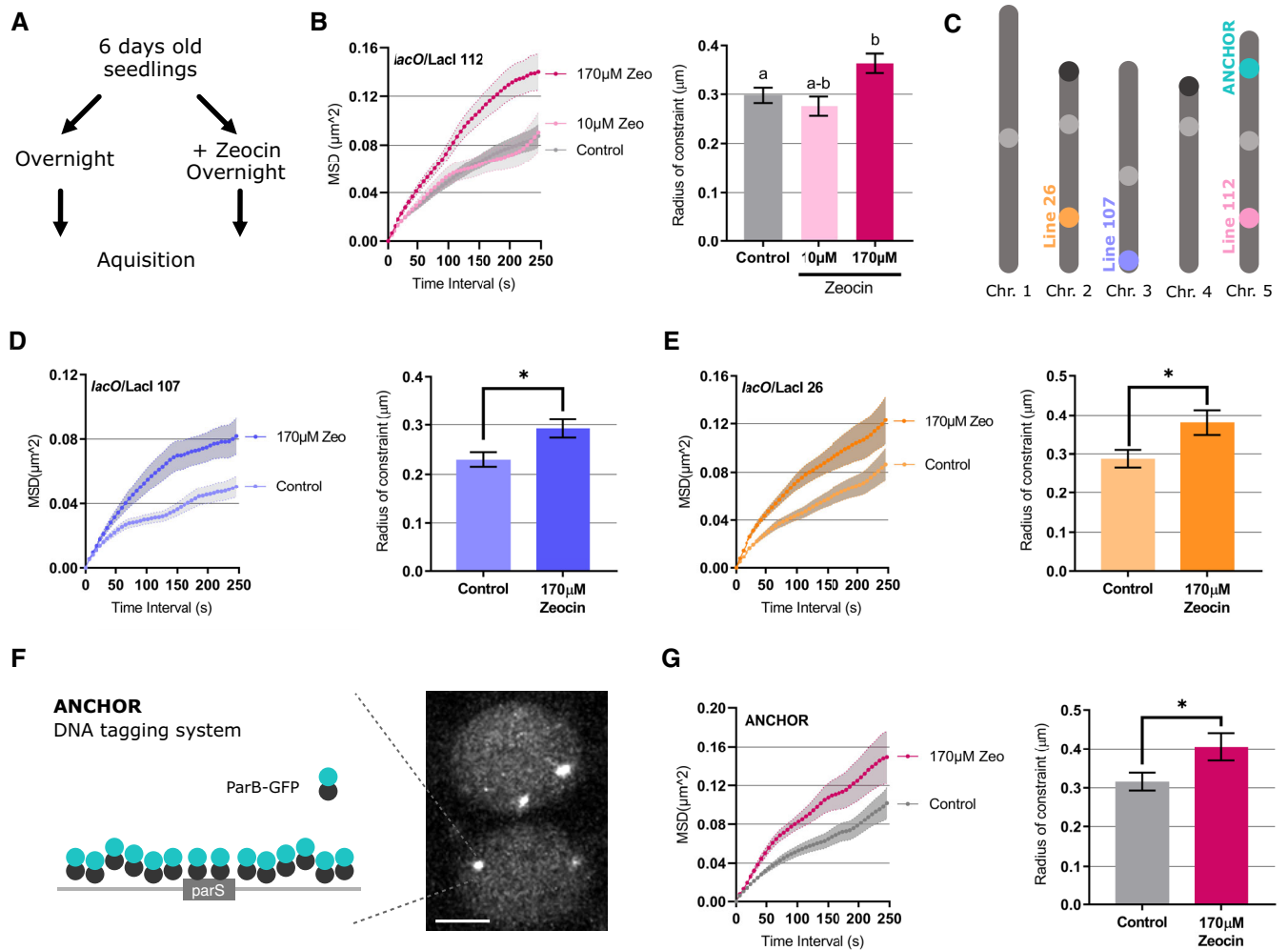


Figure 2. DNA damage increases chromatin mobility.

- A** Scheme illustrating the experimental setup for *Arabidopsis* seedling treatment.
- B** Left: MSD analysis of *lacO/LacI* line 112 based on time-lapse experiments of nuclei in different zeocin (Zeo) concentrations. Control ($n = 116$ nuclei); 10 μM ($n = 97$ nuclei); 170 μM ($n = 93$ nuclei). Right: Radius of constraint was calculated from MSD curves. Values represent means \pm SEM. Letters indicate one-way ANOVA followed by Bonferroni's correction ($P < 0.05$).
- C** Chromosomal positions of *lacO/LacI* lines as reported previously (Matzke *et al.*, 2010, 2019). Line 26, line 107, and line 112 are respectively inserted in chromosomes 2, 3, and 5. The ANCHOR construct is inserted in chromosome 5. The NORs are marked as black circles and centromeres as light gray circles.
- D** Left: MSD analysis of *lacO/LacI* line 107 based on time-lapse experiments of nuclei in control conditions and plants treated with 170 μM zeocin. Control ($n = 53$ nuclei), 170 μM zeocin ($n = 48$ nuclei). Right: Radius of constraint calculated from MSD curves. Values represent means \pm SEM. Student's *t*-test, $*P < 0.05$.
- E** Left: MSD analysis of *lacO/LacI* line 26 based on time-lapse experiments of nuclei upon zeocin. Control ($n = 52$ nuclei), 170 μM zeocin ($n = 52$ nuclei). Right: Radius of constraint calculated from MSD curves. Values represent means \pm SEM. Student's *t*-test, $*P < 0.05$.
- F** Left: Schematic representation of the ANCHOR system. *parS*-ParB:GFP interactions and oligomerization along the flanking genomic region. ParB-GFP can directly bind to *parS* sequence as a dimer and along the flanking genomic region. Right: Representative image of epidermis nuclei in the division zone. Scale bar, 5 μm .
- G** Left: MSD analysis of ANCHOR line based on time-lapse experiments of nuclei upon zeocin treatment. Control ($n = 54$ nuclei), 170 μM zeocin ($n = 22$ nuclei). Right: Radius of constraint calculated from MSD curves. Values represent means \pm SEM. Student's *t*-test, $*P < 0.05$.

mobility at S/G2 phase. This observation is consistent with the idea that HR is particularly relevant in G2 when sister chromatids have been synthesized and suggests that increased chromatin mobility may be important during this stage.

In yeast, as in plants, studies have shown that HR is executed mainly during S/G2 phases of the cell cycle (Ferreira, 2004; Weimer *et al.*, 2016). Because the increase in chromatin mobility upon zeocin treatment was specific to S/G2, we decided to investigate the mobility of actual break sites (DSBs) during HR. Homologous

recombination is divided into two main phases: the presynaptic phase, which includes 5'-end resection and homology search, and the synaptic phase, which includes the strand invasion for homologous strand pairing (Fig 4A; Wright *et al.*, 2018). Two main actors of HR, RAD51 and RAD54, function in the initiation of the strand invasion and at the strand exchange reaction that finalizes the repair (Solinger & Heyer, 2001). We wanted to investigate how the increase in chromatin mobility is placed in relation to these two phases. By performing an 8-h time course experiment on RAD51-GFP and

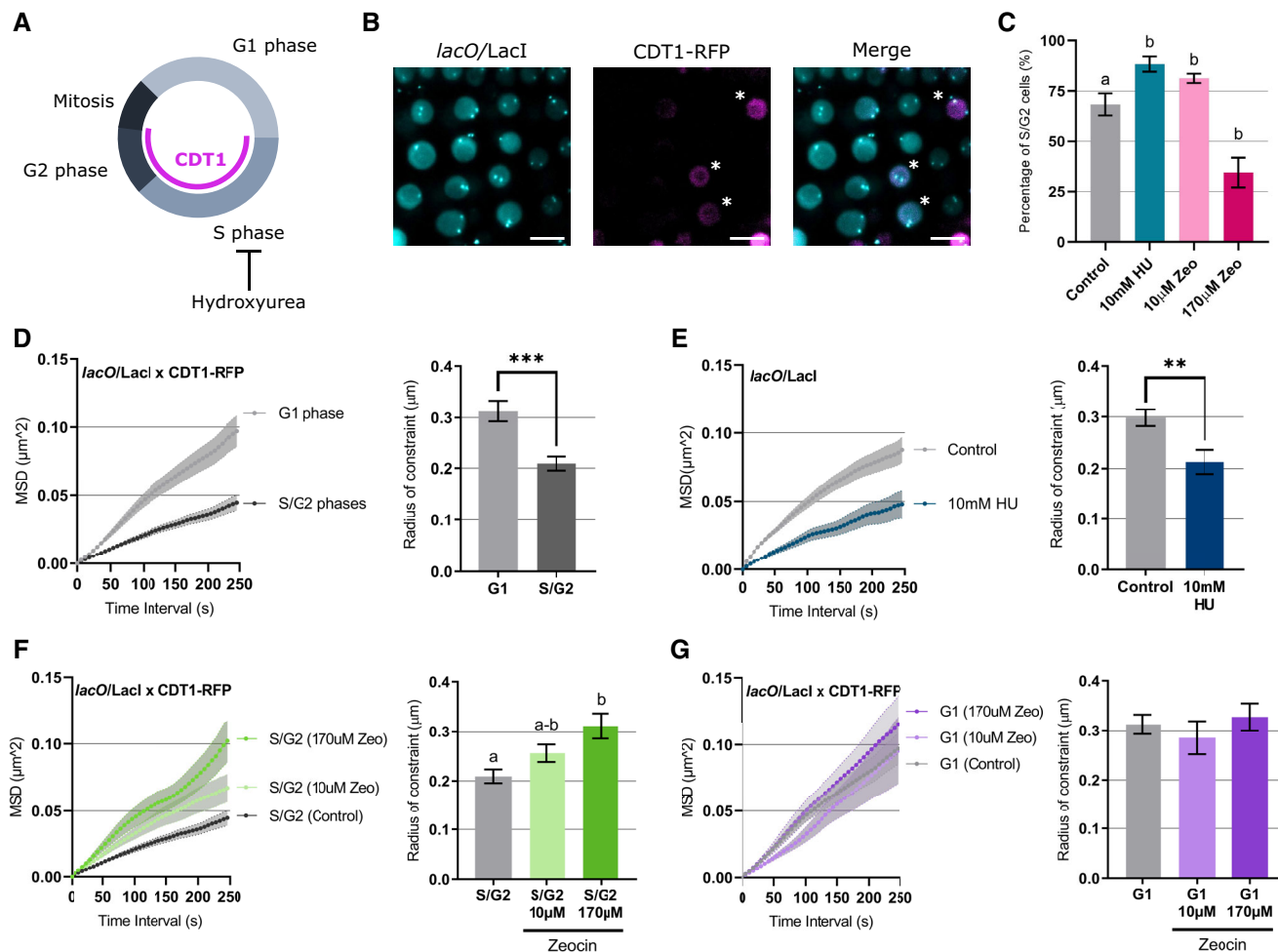


Figure 3. Chromatin mobility increases specifically during in S/G2 phase of the cell cycle in response to DNA damage.

A Schematic representation of cell cycle progression with the CDT1-RFP signal displayed in S/G2 phase.
 B Representative images of *Arabidopsis* nuclei from *lacO/LacI* line 112 crossed with CDT1-RFP. *lacO/LacI* (cyan) CDT1-RFP (magenta). Stars represent cells in S/G2. Scale bar, 10 μ m.
 C Percentage of cells in S/G2 phase per root in control conditions and upon 10 μ M hydroxyurea (HU), 10 and 170 μ M zeocin (Zeo). Values represent means \pm SEM. Letters indicate one-way ANOVA followed by Bonferroni's correction ($P < 0.05$).
 D–G MSD curves and corresponding Rc histograms for *lacO/LacI* line112: (D) in G1 nuclei ($n = 62$ nuclei) and nuclei in S/G2 phase ($n = 67$ nuclei); (E) upon 10 μ M HU treatment ($n = 28$ nuclei); Control ($n = 116$ nuclei); (F) in S/G2 cells upon different zeocin concentrations (10 μ M ($n = 60$ nuclei); 170 μ M ($n = 49$ nuclei)); Control ($n = 67$ nuclei); (G) in G1 cells upon different zeocin concentrations (10 μ M ($n = 35$ nuclei); 170 μ M ($n = 50$ nuclei)); Control ($n = 62$ nuclei). Values represent means \pm SEM. Student's *t*-test, ** $P < 0.01$ *** $P < 0.001$. Letters indicate one-way ANOVA followed by Bonferroni's correction ($P < 0.05$).

RAD54-YFP lines after induction of damage with 10 μ M zeocin, we were able to visualize the appearance of foci with accumulations of these proteins at DSB sites in the nucleus (Fig 4B and C). The tagged version of RAD51 forms the nucleofilament at DSBs but is defective in recombination and repair (Kobayashi *et al*, 2014). This defect leads to very high nucleoplasmic fluorescence with high zeocin concentrations thereby preventing individual foci from being visualized. Therefore, for these experiments, a low concentration of zeocin (10 μ M) was required. RAD51-GFP foci were formed approximately 1 h 30 min after DSB induction, whereas RAD54-YFP foci appeared later, at around 5 h after treatment (Fig 4B). From this experiment, we can infer that RAD51 interacts first with DSBs, while RAD54 comes in later. To investigate the mobility of foci tagged with these proteins, we treated RAD51-GFP and RAD54-YFP plants with 10 μ M

zeocin (Fig 4C). The MSD analysis revealed that only RAD51 showed significantly higher mobility than *lacO/LacI* foci (Fig 4D), showing that high mobility levels seem to happen at early HR stages. Additionally, the high levels of mobility observed with RAD51-GFP could be due to the fact that these correspond to DSB sites, whereas *lacO/LacI* foci mobility most likely corresponds to measurements at undamaged loci. RAD54 foci mobility however seemed to be at the level of *lacO/LacI* at 10 μ M zeocin (Fig 4D). Previous studies have shown that RAD54 foci relocate to the nuclear periphery after γ -irradiation (Hirakawa & Matsunaga, 2019). Therefore, our MSD results for RAD54 may correspond to a mixture of foci located at the nuclear periphery and non-periphery. To test if RAD54 at the different nuclear compartments behaved differently, we determined the MSD for RAD54 foci at these two nuclear locations (Fig 4E). The

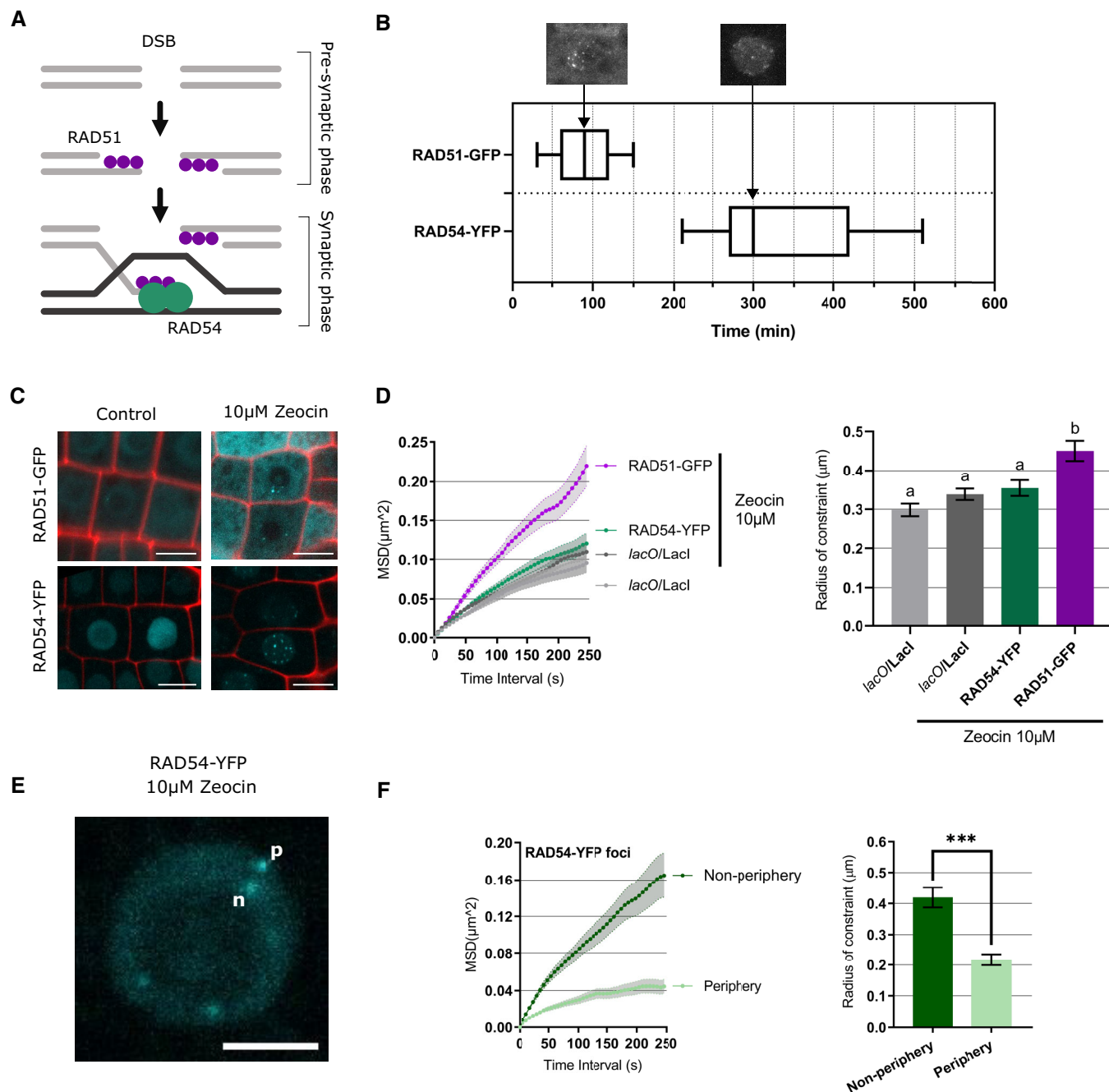


Figure 4. The mobility of DSB sites via tagged HR factors.

- A** Schematic representation of the critical steps of homologous recombination. RAD51 (purple) assembles onto the single-stranded DNA (ssDNA) formed after the resection of DNA double-strand break (DSB) ends to form a filament, which is known as the presynaptic filament. After searching for DNA homologous sequence, the presynaptic filament binds the DNA template to form the synaptic structure with RAD54. The ssDNA invades the homologous region in the duplex to form a DNA joint, known as the displacement (D)-loop promoted by Rad54 (green).
- B** Time-lapse experiment of the formation of RAD51-GFP and RAD54-YFP foci in *Arabidopsis* nuclei, imaged every 30 min. Timeline of RAD51 and RAD54 foci formation for 8 h. The middle line in the box shows the mean, and the whiskers represent the standard error. At least four roots were counted for each line.
- C** Representative images of root epidermal cells showing foci formation in RAD51-GFP and RAD54-YFP plants after 10 µM zeocin treatment for 48 h. PI staining (red). Scale bar, 10 µm.
- D** Left: MSD analysis of RAD51-GFP ($n = 64$ nuclei) and RAD54-YFP ($n = 64$ nuclei) foci and *lacO/LacI* (line112; $n = 109$ nuclei) plants upon 10 µM zeocin. Right: Radius of constraint calculated from MSD curves. Values represent means \pm SEM. Letters indicate one-way ANOVA followed by Bonferroni's correction ($P < 0.05$)
- E** Representative image of a root epidermal nucleus with RAD54-YFP foci located on the nuclear periphery (p) and non-periphery (n). Scale bar, 5 µm.
- F** Left: MSD analysis of RAD54 foci in the periphery ($n = 24$ nuclei) and non-periphery ($n = 30$ nuclei) upon 10 µM zeocin. Right: Radius of constraint calculated from MSD curves. Values represent means \pm SEM. Student's *t*-test, *** $P < 0.001$.

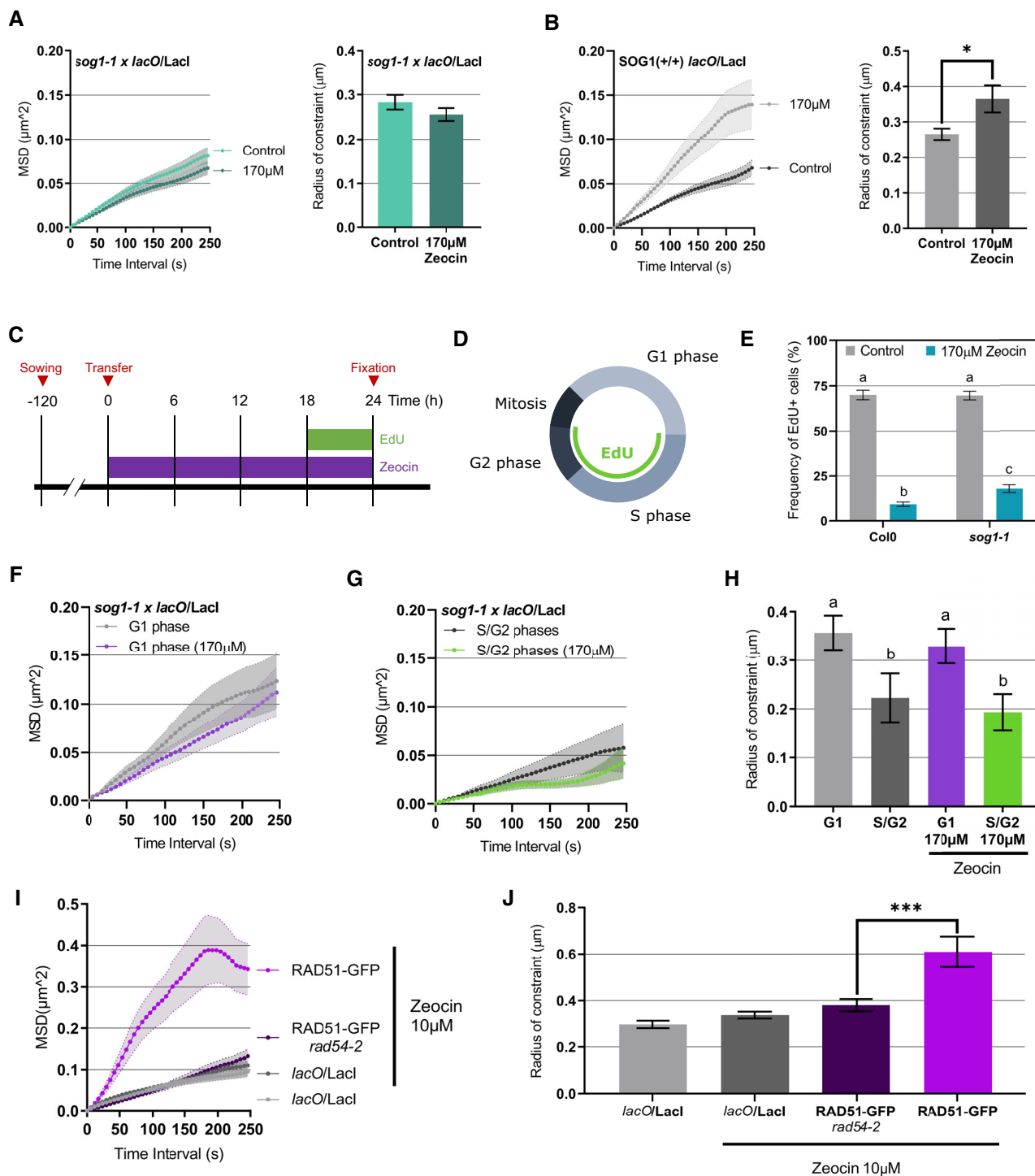


Figure 5.

results showed that non-peripheral RAD54 foci have much higher mobility than the foci at the periphery (Fig 4F), revealing that RAD54 foci can have mobilities similar to those of RAD51. Moreover, these results highlighted that large changes in DSB site mobility occur during the repair process—a strong increase in DSB mobility is observed in the early HR phase, with a subsequent drastic drop in mobility associated with the relocation of DSBs to the nuclear periphery. This

relocation to the nucleus periphery has been associated with different possible roles—to bring homologous sequences together, thereby reducing the 3D search to a 2D scale (Seeber & Gasser, 2017); or due to the fact that the repair machinery may specifically interact with nucleopores (Nagai *et al*, 2008). These observations support the hypothesis that higher DNA movement is induced at early steps of HR presumably to facilitate the 3D search.

Figure 5. SOG1 and RAD54 regulate mobility in response to DNA damage.

- A Left: MSD analysis of *Arabidopsis lacO/LacI* line 112 crossed with *sog1-1* (Control ($n = 83$ nuclei); 170 μM zeocin ($n = 91$ nuclei)). Right: Radius of constraint calculated from MSD curves.
- B Left: MSD analysis of $\text{SOG1}^{+/+}$ *lacO/LacI* progeny from crossing with *sog1-1* (Control ($n = 59$ nuclei); 170 μM zeocin ($n = 29$ nuclei)). Right: Radius of constraint calculated from MSD curves.
- C Schematic representation of the experimental setup for EdU labeling.
- D Schematic representation of cell cycle progression, with the EdU signal displayed in S/G2 phase.
- E The proportion of EdU-labeled cells in root tips of Col-0 and *sog1-1*, in control conditions and upon treatment with 170 μM zeocin. For each condition, between 5 and 6 roots were analysed ($n =$ more than 50 nuclei).
- F MSD analysis of G1 cells from *lacO/LacI* line 112 crossed with *sog1-1* mutant in control conditions ($n = 23$ nuclei) and in plants treated with 170 μM zeocin ($n = 25$ nuclei).
- G MSD analysis of cells in S/G2 from *lacO/LacI* line 112 crossed with *sog1-1* (Control ($n = 10$ nuclei); 170 μM zeocin ($n = 12$ nuclei)).
- H Radius of constraint calculated from MSD curves depicted in F and G.
- I MSD analysis for RAD51-GFP foci in wild-type plants ($n = 14$ nuclei), RAD51-GFP foci in *rad54-2* mutant background ($n = 31$ nuclei) and *lacO/LacI* (line112; $n = 109$ nuclei) plants treated with 10 μM zeocin.
- J Radius of constraint calculated from MSD curves depicted in I.

Data information: Values represent means \pm SEM. Student's *t*-test, * $P < 0.05$, *** $P < 0.001$. Letters indicate one-way ANOVA followed by Bonferroni's correction ($P < 0.05$).

Tracking chromatin movement, using DNA labeling tools and HR reporter lines, showed an increase in mobility upon DNA damage. Next, we wanted to determine whether the increase in mobility was actively regulated by the DDR pathway. For that, we quantified *lacO/LacI* (line 112) mobility in *sog1-1* mutant, in which DDR is abolished. MSD analysis in *sog1-1* mutant revealed no increase in mobility upon treatment with high zeocin concentration, indicating that the increase of mobility seen in the WT ($\text{SOG1}^{+/+}$ progeny from the F1) was dependent on SOG1 and thus on DDR activation (Fig 5A and B). However, it is important to rule out that the lack of response to zeocin treatment was not due to a change in the cell cycle dynamics in this mutant. Indeed, in *sog1-1* the cell cycle arrest upon DNA damage is compromised (Yi *et al.*, 2014; Chen *et al.*, 2017; Mahapatra & Roy, 2021) and a loss of G1-arrested cells could potentially explain the results observed. We used EdU staining to check if, under our zeocin treatment conditions, *sog1-1* cells were not being arrested in G1 (Fig 5C–E; Appendix Fig S7). The results showed that also in *sog1-1* there is a substantial reduction in EdU staining upon zeocin treatment, indicating that cells are also being accumulated at G1 although to a lesser extent than in the WT. We, therefore, decided to further analyze chromatin mobility in G1 and S/G2 in *sog1-1* mutant. Given the complexity of this line, with several T-DNA insertions, instead of crossing it with CDT1a::RFP reporter we used nuclear area as a proxy for cell cycle stage taking as a reference CDT1 labeling (Appendix Fig S8). This analysis revealed that in *sog1-1* at both G1 and S/G2 stages of the cell cycle, there is no increase in mobility upon zeocin treatment (Fig 5F–H). These results demonstrate that SOG1 is required for the increase in chromatin mobility induced by zeocin treatment, indicating that this phenomenon is actively regulated during the early steps of the response to DNA damage and not a physical by-product from extensive DNA “fragmentation.” Previous studies in yeast and animals have shown that increased chromatin mobility is dependent on the protein kinases ATM/ATR (Dion *et al.*, 2012; Becker *et al.*, 2014), which have a primary role in DDR and promote SOG1 activation (Yoshiyama *et al.*, 2009, 2013a). It will now be relevant to define which molecular players downstream of SOG1 are involved in the increased chromatin mobility in plants. RAD51 and RAD54 are two factors that act downstream of SOG1 and are essential for HR. RAD51 forms filaments on ssDNA, while RAD54 is an Snf2-type ATPase with translocase activity. As recruitment of

RAD51 to DSBs does not depend on RAD54 (Hernandez Sanchez-Rebato *et al.*, 2021), we generated a RAD51-GFP line containing a mutation on RAD54 (*rad54-2*) and followed the dynamics of RAD51 foci on this mutant line. *Rad54-2* mutation resulted in a significant decrease in RAD51-GFP foci mobility to levels similar to those of undamaged sites (Fig 5I and J). Thus, we concluded that this important component of the HR machinery (RAD54) is involved in DSB mobility in plants. These results are in agreement with studies in yeast (Dion *et al.*, 2013), which show that the mobility of damaged DNA increases in a RAD54-dependent manner. Whether RAD54 has a role beyond DSB mobility and is required for global changes in chromatin mobility remains to be addressed. However, previous studies in *Arabidopsis* have shown the involvement of RAD54 in pairing of *lacO/LacI* foci (Hirakawa *et al.*, 2015), suggesting a potential role at the global chromatin level.

Our analysis of global chromosome and double-strand break (DSB) site mobility, using *lacO/LacI* lines and RAD51-GFP and RAD54-YFP reporters, has revealed that an increase in chromatin mobility occurs in response to DNA damage in *Arabidopsis*. Similar responses have been observed in yeast and animal cells, pointing towards a general mechanism of response to DSBs across kingdoms (Dimitrova *et al.*, 2008; Dion *et al.*, 2012; Krawczyk *et al.*, 2012; Miné-Hattab & Rothstein, 2012). Although the exact function of such an increase in mobility has not been fully uncovered, some studies suggest it could increase the probability of an encounter between the break and the repair template (Barzel & Kupiec, 2008; Gehlen *et al.*, 2011). However, this hypothesis needs to be tested with experiments that directly link chromatin mobility and HR efficiency. Even though the DNA repair machinery is highly conserved among eukaryotes, some of the most important regulators in animals, such as the tumor suppressor p53, are absent in plants. Its function is instead served by the plant-specific DDR master regulator SOG1. Interestingly, we have been able to show that in plants the increase in chromatin mobility is dependent on SOG1 function. These results suggest that the increase in chromatin mobility was conserved in evolution, as a response to DNA damage potentially through the action of different molecular players. A deeper understanding of the mechanisms downstream of SOG1 directly responsible for the increased chromatin mobility upon DNA damage in plants is needed in future studies.

Material and Methods

Plant lines and growth conditions

Mutants and transgenic lines used in this study come from the following sources: *sog1-1* (Yoshiyama et al, 2009), *rad54-2* (Hernandez Sanchez-Rebato et al, 2021), RAD51-GFP (Da Ines et al, 2013), RAD54-eYFP (Hirakawa & Matsunaga, 2019), Cytrap line (Yin et al, 2014), *lacO/LacI* lines (Matzke et al, 2010), and ANCHOR line (Meschichi et al, 2021). All mutants and transgenic lines are in Columbia background.

To visualize S/G2 cells in the *lacO/LacI* line 112, we crossed this line with Cytrap line. The resulting F₂ plants were selected on MS plates containing 50 mg/l of kanamycin (Sigma-Aldrich, catalog number K1377). Because the G2/M-marker CYCB1;1 is strongly expressed during DNA damage (Culligan et al, 2006), the selected F₂ were screened only for LacI-GFP and CDT1a-RFP.

Seeds were sterilized in 5% v/v sodium hypochlorite for 5 min and rinsed three times in sterile distilled water. Seeds were stratified at 4°C for 48 h in the darkness. Seeds were then plated on Murashige and Skoog (MS) solid medium and then grown in 16/8 h light/dark cycles at 22°C in vertically oriented Petri dishes. The roots were observed after 6 to 7 day of incubation, depending on the experiment.

Genotoxic treatment

To induce DNA damage response, 5- to 6-day-old seedlings were transferred in solid MS medium without or with 100 μM mitomycin C (MMC); 2, 10, 50, 100, or 170 μM zeocin or 10 mM hydroxyurea (HU) and treated for 2, 6, or 24 h. Each chemical was obtained respectively from Fisher Scientific (catalog number 2980501), Invitrogen (catalog number R25001), and Sigma-Aldrich (catalog number H8627-1G).

Microscopy

For root staining with propidium iodide (PI), 6- to 7-day-old seedlings were mounted in water between slide and coverslip and sealed with 0.12-mm-thick SecureSeal Adhesive tape (Grace Bio-Labs) to reduce drift drying during imaging.

For EdU staining and immunostaining, samples were imaged using a Zeiss LSM800 inverted microscope, with a 63× water objective (1.20 NA) and Microscopy Camera AxioCam 503 mono; fluorescence of Alexa488 was detected using a 450–490 nm excitation filter and by collecting the signal between 505–550 nm. For DAPI, an excitation filter 335–383 nm was used, and the signal was detected between 420–470 nm. For RAD51-GFP and RAD54-YFP time course experiments, samples were imaged using a Zeiss LSM780 inverted microscope, with 63x water objective (1.20 NA). Imaging was performed every 30 min for 8 h. Z-stacks of 19.5 μm size and 0.5 μm z-step were collected. Image size was 595 x 512 pixels with a zoom factor of 2x. RAD51-GFP and RAD54-YFP signals were detected using a 488 nm excitation line and collected between 493–598 nm.

Mean square displacement

For all MSD experiments, time-lapse imaging was performed every 6 s, taking a Z-stack of 3 μm spread through 1 μm slices for 5 min,

with a 512 × 512 pixels format with a 1–2× zoom factor. All images were analyzed using Fiji software (NIH, Bethesda, MD, <http://rsb.info.nih.gov/ij/>; Sage et al, 2005) and with the plugin SpotTracker 2D (obtained from <http://bigwww.epfl.ch/sage/soft/spottracker/>). All our time series were corrected for XY drift and nuclear movement using the plugins Stackreg and SpotTracker 2D, respectively. All the details of our image analyses pipeline were done as described in Meschichi and Rosa (2021).

Expression analysis using real-time RT-PCR (qPCR)

Seedlings grown for 7 days were harvested, and total RNA was extracted using the TRIzol reagent (Invitrogen). A total of 1 μg of RNA was treated with TURBO DNase (Life Technologies) and used for cDNA synthesis (Superscript IV; Life Technologies). The resulting cDNA was diluted 10 times and used for quantitative PCR using a Bio-Rad iCycler Thermal Cycler iQ5 Multicolor Real-Time and HOT FIREPol® EvaGreen® qPCR Mix Plus (Solis Biodyne). For data normalization, the data were first normalized to the PP2A2 reference gene, and the values from two independent samples were normalized to the average Delta Ct value Col-0 level or control condition (2^{-ΔΔCt} Method). The final values presented are given as the mean ± SD from three independent samples. Minus RT (no reverse transcriptase control) controls were set up to make sure the values reflect the level of RNA and not DNA contamination. The standard Student's *t*-test was used to determine the statistical significance of the results. The primers used are listed in Appendix Table S1.

EdU labeling

Five-day-old seedlings were grown on solid medium, treated with 170 μM zeocin for 24 h and incubated on solid medium containing 20 μM EdU and 170 μM zeocin during the last 6 h before imaging. Roots were fixed in 4% paraformaldehyde (PFA) for 30 min and washed three times with 1 × PBS. The roots were transferred to slide and covered by a glass cover slip, then squashed, and immediately dipped in liquid nitrogen for few seconds. The cover slips were removed, and the roots were left to dry at room temperature for 30 min. The samples were washed with PBS + BSA (Bovine Serum Albumin) 3% (w/v) and incubated with a ClickIt Buffer (PBS 1× pH7.4, CuSO₄ 100 mM, Ascorbate 1 M, Alexia fluor azide, 2 μM) solution in the dark for 15 min. Samples were washed once in 1× PBS + BSA 3%, followed by DAPI staining for 15 min in the dark. Samples were washed twice with PBS 1× pH 7.4 and mounted in vectashield (Vector Laboratories).

Immunofluorescence

Roots were fixed in 4% PFA for 30 min and washed three times with 1 × PBS. The roots were transferred to slides and covered by a glass coverslip, then squashed, and immediately dipped in liquid nitrogen for few seconds. The coverslips were removed, and the roots were left to dry at room temperature for 30 min. Samples were then rinsed three times with 1× PBS solution and incubated with the enzyme mix (5% Driselase, 2.5% Cellulase, 5% Macerozyme in 1× PBS) for 15 min in a humid chamber at 37°C. Each slide was incubated overnight at 4°C with 50 μl rabbit, anti-plant γ-H2AX antiserum diluted 1:500 in fresh blocking buffer (0.5% BSA, in 1× PBS) and washed three times in 1×

PBS solution. Slides were incubated for 2 h in a humid chamber at 37°C in 50 µl blocking buffer consisting of Alexa 488-conjugated goat anti-rabbit (1:1,000 Agrisera, catalog number: AS09633) secondary antibodies. Finally, slides were washed three times for 5 min in blocking buffer followed by DAPI staining for 15 min in the dark. Samples were washed twice with PBS 1× and mounted in vectashield (Vector Laboratories). Three-dimensional image stacks were captured, and γ-H2AX foci were counted manually.

The primary antibody was provided by C. White and used as performed in a previous study (Charbonnel *et al*, 2010).

Statistical analysis

For statistical analysis, we used the GraphPad Prism 8.3 software. Data sets were tested for normality using the Shapiro–Wilk test. Statistical significance was determined by using the standard Student's *t*-test (two-tailed) and one-way ANOVA (multiple comparisons with Bonferroni correction). All experiments were performed in several nuclei as mentioned in figure legends.

Data availability

Data from this study are not deposited in external repositories, but can be requested from the corresponding author.

Expanded View for this article is available [online](#).

Acknowledgements

We thank Susan Gasser and Anis Cheblal for the SpotTracking and Excel Macro, Charles White for RAD51-GFP line, Anne Britt for the *sog1-1* mutant, Sashihiro Matstunaga for RAD54-eYFP line, Masaaki Umeda and Shiori Aki for the Cytrap line and Confocal Microscopy Platform from SLU, Uppsala, Sweden. We thank Marion Orsucci for help with the statistical analysis. We thank Lauriane Simon for comments on the manuscript. We would like to thank COST ACTION CA16212 INDEPTH for the inputs and comments. AM and SR were supported by the Swedish Research Council (Vetenskapsrådet) grant number 2018-04101 and Knut and Alice Wallenberg Foundation (KAW 2019-0062). FP is supported by the “Laboratoires d’Excellences (LABEX)” TULIP (ANR-10-LABX-41) and/or by the “École Universitaire de Recherche (EUR)” TULIP-GS (ANR-18-EURE-0019). AS and LZ were supported by Carl Tryggers Stiftelse (18:350), Marie Skłodowska-Curie Individual Fellowships (MSCA-IF 101032710), and the Swedish Research Council (Vetenskapsrådet) grant number 2018-04214.

Author contributions

Anis Meschichi: Conceptualization; formal analysis; investigation; writing – original draft; writing – review and editing. **Lihua Zhao:** Investigation; formal analysis. **Svenja Reeck:** Investigation; formal analysis. **Charles White:** Methodology; writing – review and editing. **Olivier Da Ines:** Methodology; writing – review and editing. **Adrien Sicard:** Conceptualization; supervision. **Frederic Pontvianne:** Investigation; methodology. **Stefanie Rosa:** Conceptualization; formal analysis; supervision; funding acquisition; investigation; writing – original draft; project administration; writing – review and editing.

Disclosure and competing interest statement

ANCHOR system is the property of NeoVirTech SAS, Toulouse, France. Any request of use should be addressed to contact@neovirtech.com.

References

- Arai R, Sugawara T, Sato Y, Minakuchi Y, Toyoda A, Nabeshima K, Kimura H, Kimura A (2017) Reduction in chromosome mobility accompanies nuclear organization during early embryogenesis in *Caenorhabditis elegans*. *Sci Rep* 7: 3631
- Armstrong SJ, Franklin FC, Jones GH (2001) Nucleolus-associated telomere clustering and pairing precede meiotic chromosome synapsis in *Arabidopsis thaliana*. *J Cell Sci* 114: 4207–4217
- Barzel A, Kupiec M (2008) Finding a match: how do homologous sequences get together for recombination? *Nat Rev Genet* 9: 27–37
- Becker A, Durante M, Taucher-Scholz G, Jakob B (2014) ATM alters the otherwise robust chromatin mobility at sites of DNA double-strand breaks (DSBs) in human cells. *PLoS One* 9: e92640
- Bourbousse C, Vegesna N, Law JA (2018) SOG1 activator and MYB3R repressors regulate a complex DNA damage network in *Arabidopsis*. *Proc Natl Acad Sci U S A* 115: E12453–E12462
- Chang HHY, Pannunzio NR, Adachi N, Lieber MR (2017) Non-homologous DNA end joining and alternative pathways to double-strand break repair. *Nat Rev Mol Cell Biol* 18: 495–506
- Charbonnel C, Gallego ME, White CI (2010) Xrcc1-dependent and Ku-dependent DNA double-strand break repair kinetics in *Arabidopsis* plants. *Plant J* 64: 280–290
- Cheblal A, Challa K, Seeber A, Shimada K, Yoshida H, Ferreira HC, Amitai A, Gasser SM (2020) DNA damage-induced nucleosome depletion enhances homology search independently of local break movement. *Mol Cell* 80: 311–326.e4
- Chen P, Takatsuka H, Takahashi N, Kurata R, Fukao Y, Kobayashi K, Ito M, Umeda M (2017) *Arabidopsis* R1R2R3-Myb proteins are essential for inhibiting cell division in response to DNA damage. *Nat Commun* 8: 635
- Cools T, Iantcheva A, Maes S, Van den Daele H, De Veylder L (2010) A replication stress-induced synchronization method for *Arabidopsis thaliana* root meristems. *Plant J* 64: 705–714
- Culligan KM, Robertson CE, Foreman J, Doerner P, Britt AB (2006) ATR and ATM play both distinct and additive roles in response to ionizing radiation. *Plant J* 48: 947–961
- Da Ines O, Degroote F, Goubely C, Amiard S, Gallego ME, White CI (2013) Meiotic recombination in *Arabidopsis* is catalysed by DMC1, with RAD51 playing a supporting role. *PLoS Genet* 9: e1003787
- Dimitrova N, Chen Y-CM, Spector DL, de Lange T (2008) 53BP1 promotes non-homologous end joining of telomeres by increasing chromatin mobility. *Nature* 456: 524–528
- Dion V, Kalck V, Horigome C, Towbin BD, Gasser SM (2012) Increased mobility of double-strand breaks requires Mec1, Rad9 and the homologous recombination machinery. *Nat Cell Biol* 14: 502–509
- Dion V, Kalck V, Seeber A, Schleker T, Gasser SM (2013) Cohesin and the nucleolus constrain the mobility of spontaneous repair foci. *EMBO Rep* 14: 984–991
- Ferreira MG (2004) Two modes of DNA double-strand break repair are reciprocally regulated through the fission yeast cell cycle. *Genes Dev* 18: 2249–2254
- Franz P, de Jong JH, Lysak M, Castiglione MR, Schubert I (2002) Interphase chromosomes in *Arabidopsis* are organized as well defined chromocenters from which euchromatin loops emanate. *Proc Natl Acad Sci U S A* 99: 14584–14589
- Fulcher N, Sablowski R (2009) Hypersensitivity to DNA damage in plant stem cell niches. *Proc Natl Acad Sci U S A* 106: 20984–20988

- Gehlen LR, Gasser SM, Dion V (2011) How broken DNA finds its template for repair: a computational approach. *Prog Theor Phys Suppl* 191: 20–29
- van Gent DC, Hoeijmakers JHJ, Kanaar R (2001) Chromosomal stability and the DNA double-stranded break connection. *Nat Rev Genet* 2: 196–206
- Goldfarb T, Lichten M (2010) Frequent and efficient use of the sister chromatid for DNA double-strand break repair during budding yeast meiosis. *PLoS Biol* 8: 10–12
- Hernandez Sanchez-Rebato M, Bouatta AM, Gallego ME, White CI, Da Ines O (2021) RAD54 is essential for RAD51-mediated repair of meiotic DSB in *Arabidopsis*. *PLoS Genet* 17: e1008919
- Hirakawa T, Matsunaga S (2019) Characterization of DNA repair foci in root cells of *Arabidopsis* in response to DNA damage. *Front Plant Sci* 10: 990
- Hirakawa T, Katagiri Y, Ando T, Matsunaga S (2015) DNA double-strand breaks alter the spatial arrangement of homologous loci in plant cells. *Sci Rep* 5: 11058
- Hirakawa T, Hasegawa J, White CI, Matsunaga S (2017) RAD54 forms DNA repair foci in response to DNA damage in living plant cells. *Plant J* 90: 372–382
- Horigome C, Dion V, Seeber A, Gehlen LR, Gasser SM (2015) Visualizing the spatiotemporal dynamics of DNA damage in budding yeast. *Methods Protoc* 1292: 77–96
- Hustedt N, Durocher D (2017) The control of DNA repair by the cell cycle. *Nat Cell Biol* 19: 1–9
- Jackson SP (2002) Sensing and repairing DNA double-strand breaks. *Carcinogenesis* 23: 687–696
- Johnson RD, Jasin M (2000) Sister chromatid gene conversion is a prominent double-strand break repair pathway in mammalian cells. *EMBO J* 19: 3398–3407
- Kawarazaki T, Kimura S, Iizuka A, Hanamata S, Nibori H, Michikawa M, Imai A, Abe M, Kaya H, Kuchitsu K (2013) A low temperature-inducible protein AtSRC2 enhances the ROS-producing activity of NADPH oxidase AtRbohF. *Biochim Biophys Acta Mol Cell Res* 1833: 2775–2780
- Kobayashi W, Sekine S, Machida S, Kurumizaka H (2014) Green fluorescent protein fused to the C terminus of RAD51 specifically interferes with secondary DNA binding by the RAD51-ssDNA complex. *Genes Genet Syst* 89: 169–179
- Krawczyk PM, Borovski T, Stap J, Cijssouw T, Cate RT, Medema JP, Kanaar R, Franken NAP, Aten JA (2012) Chromatin mobility is increased at sites of DNA double-strand breaks. *J Cell Sci* 125: 2127–2133
- Küpper H, Andresen E (2016) Mechanisms of metal toxicity in plants. *Metalomics* 8: 269–285
- Lee S, Seo PJ, Lee H-J, Park C-M (2012) A NAC transcription factor NTL4 promotes reactive oxygen species production during drought-induced leaf senescence in *Arabidopsis*. *Plant J* 70: 831–844
- Li X, Heyer WD (2008) Homologous recombination in DNA repair and DNA damage tolerance. *Cell Res* 18: 99–113
- Mahapatra K, Roy S (2021) SOG1 transcription factor promotes the onset of endoreduplication under salinity stress in *Arabidopsis*. *Sci Rep* 11: 11659
- Matzke AJM, Watanabe K, van der Winden J, Naumann U, Matzke M (2010) High frequency, cell type-specific visualization of fluorescent-tagged genomic sites in interphase and mitotic cells of living *Arabidopsis* plants. *Plant Methods* 6: 2
- Matzke AJM, Lin W, Matzke M (2019) Evidence that ion-based signaling initiating at the cell surface can potentially influence chromatin dynamics and chromatin-bound proteins in the nucleus. *Front Plant Sci* 10: 1267
- Meschichi A, Rosa S (2021) Visualizing and measuring single locus dynamics in *Arabidopsis thaliana*. In *Arabidopsis protocols*, JJ Sanchez-Serrano, J Salinas (eds), pp 213–224. New York, NY: Springer US
- Meschichi A, Ingouff M, Picart C, Mirouze M, Desset S, Gallardo F, Bystricky K, Picault N, Rosa S, Pontvianne F (2021) ANCHOR: a technical approach to monitor single-copy locus localization in planta. *Front Plant Sci* 12: 677849
- Miné-Hattab J, Rothstein R (2012) Increased chromosome mobility facilitates homology search during recombination. *Nat Cell Biol* 14: 510–517
- Nagai S, Dubrana K, Tsai-Pflugfelder M, Davidson MB, Roberts TM, Brown GW, Varela E, Hediger F, Gasser SM, Krogan NJ (2008) Functional targeting of DNA damage to a nuclear pore-associated SUMO-dependent ubiquitin ligase. *Science* 322: 597–602
- Oza P, Jaspersen SL, Miele A, Dekker J, Peterson CL (2009) Mechanisms that regulate localization of a DNA double-strand break to the nuclear periphery. *Genes Dev* 23: 912–927
- Pontvianne F, Carpentier M-C, Durut N, Pavlišťová V, Jaške K, Schořová Š, Parrinello H, Rohmer M, Pikaard CS, Fojtová M et al (2016) Identification of nucleolus-associated chromatin domains reveals a role for the nucleolus in 3D organization of the *A. thaliana* genome. *Cell Rep* 16: 1574–1587
- Ries G, Buchholz G, Frohnmeyer H, Hohn B (2000) UV-damage-mediated induction of homologous recombination in *Arabidopsis* is dependent on photosynthetically active radiation. *Proc Natl Acad Sci U S A* 97: 13425–13429
- Rosa S, Ntoukakis V, Ohmido N, Pendle A, Abranches R, Shaw P (2014) Cell differentiation and development in *Arabidopsis* are associated with changes in histone dynamics at the single-cell level. *Plant Cell* 26: 4821–4833
- Ryu T, Spatola B, Delabaere L, Bowlin K, Hopp H, Kunitake R, Karpen GH, Chiolo I (2015) Heterochromatic breaks move to the nuclear periphery to continue recombinational repair. *Nat Cell Biol* 17: 1401–1411
- Sage D, Neumann FR, Hediger F, Gasser SM, Unser M (2005) Automatic tracking of individual fluorescence particles: application to the study of chromosome dynamics. *IEEE Trans Image Process* 14: 1372–1383
- Schrank BR, Aparicio T, Li Y, Chang W, Chait BT, Gundersen GG, Gottesman ME, Gautier J (2018) Nuclear ARP2/3 drives DNA break clustering for homology-directed repair. *Nature* 559: 61–66
- Seeber A, Gasser SM (2017) Chromatin organization and dynamics in double-strand break repair. *Curr Opin Genet Dev* 43: 9–16
- Seeber A, Dion V, Gasser SM (2013) Checkpoint kinases and the INO80 nucleosome remodeling complex enhance global chromatin mobility in response to DNA damage. *Genes Dev* 27: 1999–2008
- Singh A, Xu Y-J (2016) The cell killing mechanisms of hydroxyurea. *Genes* 7: 99
- Solinger JA, Heyer W-D (2001) Rad54 protein stimulates the postsynaptic phase of Rad51 protein-mediated DNA strand exchange. *Proc Natl Acad Sci U S A* 98: 8447–8453
- Weimer AK, Biedermann S, Harashima H, Roodbarkelari F, Takahashi N, Foreman J, Guan Y, Pochon G, Heese M, Van Damme D et al (2016) The plant-specific CDKB1-CYCB1 complex mediates homologous recombination repair in *Arabidopsis*. *EMBO J* 35: 2068–2086
- West CE, Waterworth WM, Sunderland PA, Bray CM (2004) *Arabidopsis* DNA double-strand break repair pathways. *Biochem Soc Trans* 32: 964–966
- Wright WD, Shah SS, Heyer W-D (2018) Homologous recombination and the repair of DNA double-strand breaks. *J Biol Chem* 293: 10524–10535
- Yi D, Kamei CLA, Cools T, Vanderauwera S, Takahashi N, Okushima Y, Eekhout T, Yoshiyama KO, Larkin J, Van den Daele H et al (2014) The *Arabidopsis* SIAMESE-RELATED cyclin-dependent kinase inhibitors SMR5 and SMR7

- regulate the DNA damage checkpoint in response to reactive oxygen species. *Plant Cell* 26: 296–309
- Yin K, Ueda M, Takagi H, Kajihara T, Sugamata Aki S, Nobusawa T, Umeda-Hara C, Umeda M (2014) A dual-color marker system for *in vivo* visualization of cell cycle progression in *Arabidopsis*. *Plant J* 80: 541–552
- Yoshiyama K, Conklin PA, Huefner ND, Britt AB (2009) Suppressor of gamma response 1 (SOG1) encodes a putative transcription factor governing multiple responses to DNA damage. *Proc Natl Acad Sci U S A* 106: 12843–12848
- Yoshiyama KO, Kobayashi J, Ogita N, Ueda M, Kimura S, Maki H, Umeda M (2013a) ATM-mediated phosphorylation of SOG1 is essential for the DNA damage response in *Arabidopsis*. *EMBO Rep* 14: 817–822
- Yoshiyama KO, Sakaguchi K, Kimura S (2013b) DNA damage response in plants: Conserved and variable response compared to animals. *Biology* 2: 1338–1356
- Zhao Q, Zhou L, Liu J, Cao Z, Du X, Huang F, Pan G, Cheng F (2018) Involvement of CAT in the detoxification of HT-induced ROS burst in rice anther and its relation to pollen fertility. *Plant Cell Rep* 37: 741–757



License: This is an open access article under the terms of the [Creative Commons Attribution-NonCommercial-NoDerivs](https://creativecommons.org/licenses/by-nc-nd/4.0/) License, which permits use and distribution in any medium, provided the original work is properly cited, the use is non-commercial and no modifications or adaptations are made.